Science Advances
AAAS

advances.sciencemag.org/cgi/content/full/6/16/eaay8305/DC1

Supplementary Materials for

Electro-actuated valves and self-vented channels enable programmable flow control and monitoring in capillary-driven microfluidics

Yulieth Arango, Yuksel Temiz*, Onur Gökçe, Emmanuel Delamarche

*Corresponding author. Email: yte@zurich.ibm.com

Published 17 April 2020, *Sci. Adv.* **6**, eaay8305 (2020)
DOI: 10.1126/sciadv.aay8305

The PDF file includes:

Other Supplementary Material for this manuscript includes the following:

(available at advances.sciencemag.org/cgi/content/full/6/16/eaay8305/DC1)

Movies S1 to S8 (.mp4 format)

Supplementary Figures:

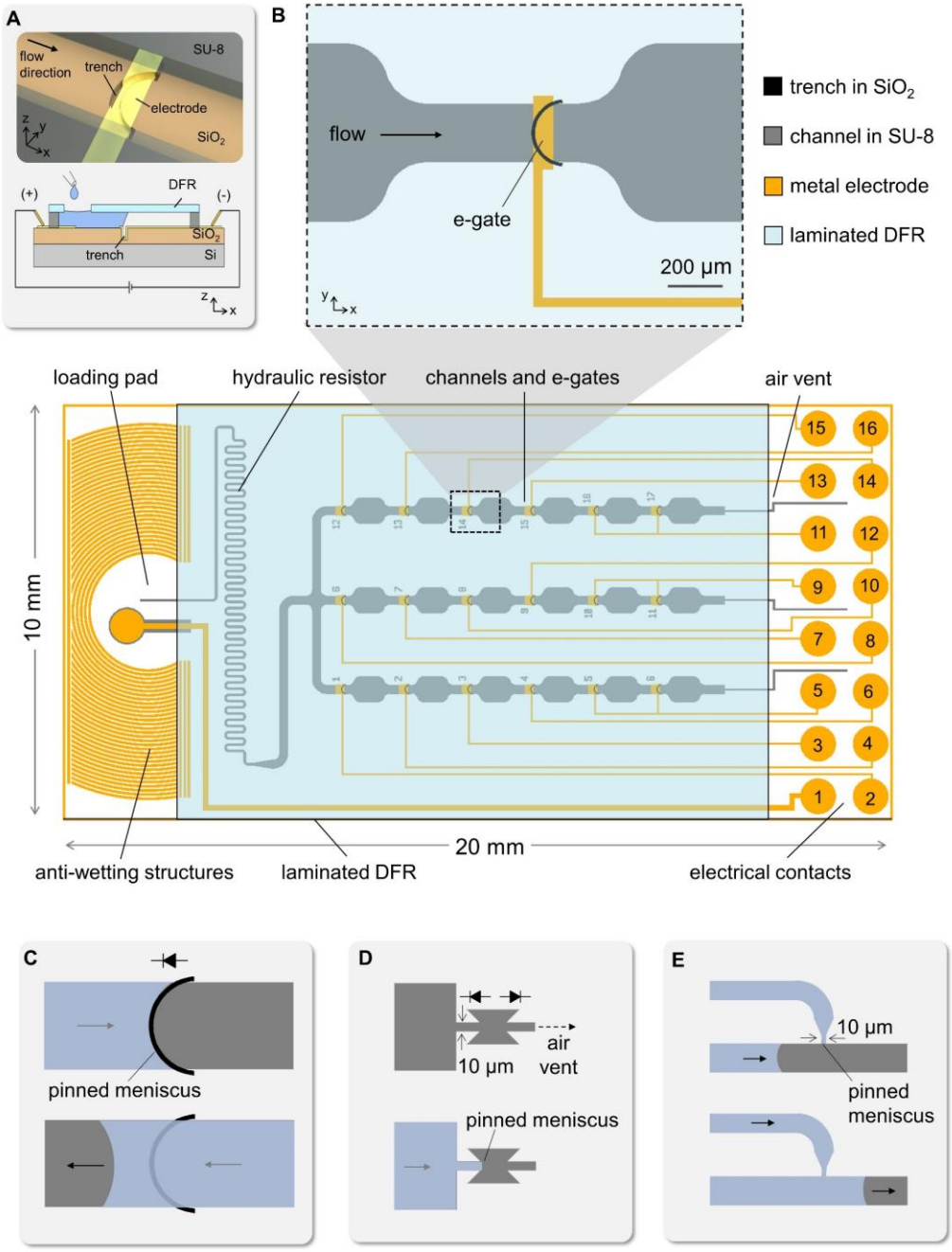

Fig. S1. Design of programmable liquid circuits implemented in capillary-driven microfluidics. (A) Operation principle of e-gates using a trench geometry where 3D-rendered (top) and cross-section (bottom) illustrations show the components and the electrical configuration. The shape of the trench is curved to semicircular geometry to improve the stability of the pinning where the trench and the sidewalls intersect, which is the point where pinning typically fails. **(B)** Example of a microfluidic chip layout comprising a loading pad, a hydraulic resistor, microfluidic channels with e-gates, and air vents to push the air out during the capillary filling of channels with the liquid. The inset shows the magnified view of an e-gate layout. A rectangular piece of dry film resist (DFR) is used to seal the chip surface, leaving the loading pad and the electrical contacts accessible from outside. Anti-wetting structures patterned around the loading pad prevent the spreading of the pipetted liquid sample. Illustrations of **(C)** "passive" e-gate trenches used as a one-way liquid valve (diode), **(D)** capillary stop valves with lateral expansions used to stop the liquid permanently before the air vent, and **(E)** capillary trigger valves where the flow of a liquid is triggered by another liquid.

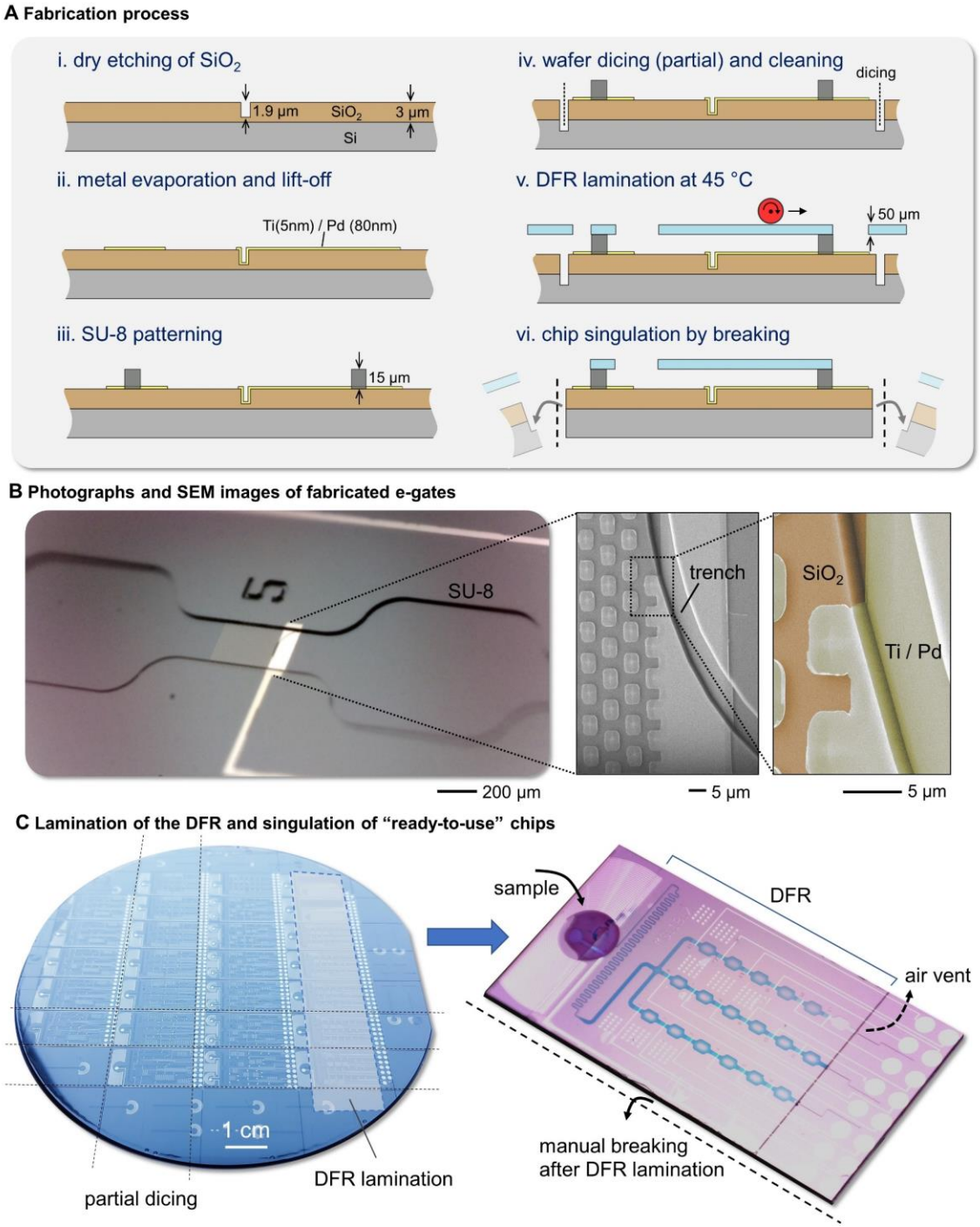

Fig. S2. Fabrication of programmable liquid circuits on a Si wafer and singulation of "ready-to-use" chips by breaking by hand. **(A)** Cross-section illustrations (not to scale) of a wafer showing the main process steps: (i) E-gate trenches are etched on a SiO_2 passivation layer using anisotropic dry etching and a photoresist mask, (ii) electrodes are patterned using e-beam evaporation and a metal lift-off process, (iii) microfluidic structures are defined by photopatterning a 15-µm-thick SU-8 layer, (iv) the wafer is partially diced (half of its initial thickness), (v) a DFR is laminated on the wafer at 45 °C to seal the chips, and (vi) sealed chips are singulated by breaking the wafer near the dicing cuts. **(B)** A photograph and SEM images of an e-gate showing the channels in SU-8, trenches in SiO_2 and the metal electrode conformally coating the trench. **(C)** On the left is a photograph of the 4-inch Si wafer after partial dicing and before DFR lamination. Rectangular strips of DFR were manually aligned to cover the microfluidic structures, leaving the liquid loading pads and electrical contacts accessible. On the right is a photograph of a singulated chip after DFR lamination, chip singulation and capillary-driven flow and electrogating of a pipetted sample. Photo credit: Yulieth Arango and Yuksel Temiz, IBM Research - Zurich

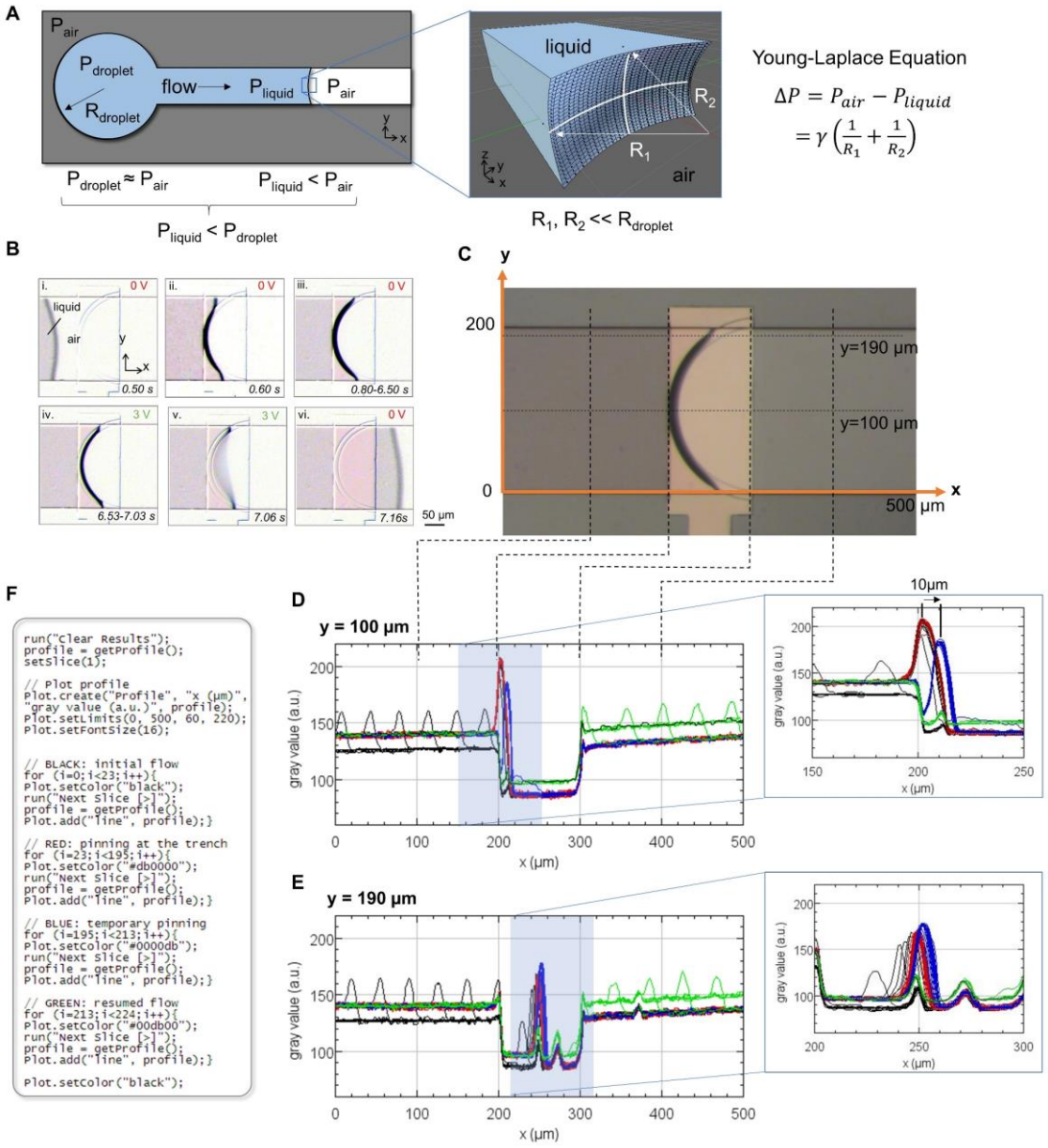

Fig. S3. Analysis of the stop-and-go flow of a liquid at an e-gate implemented in a capillary-driven microfluidic chip. (A) A simplified illustration of a capillary-driven microfluidic chip with a loading pad and a channel. The capillary pressure difference (ΔP) across the liquid-air interface is described by the Young-Laplace equation, where R_1 and R_2 are the principal radii of curvature and γ is the surface tension of the liquid. The pressure drop across the liquid-air interface of the macroscopic droplet ($R_{droplet} >> R_1, R_2$) pipetted to the loading pad and the hydrostatic pressure are negligible; therefore, $P_{air} \approx P_{droplet}$. For the case $P_{liquid}<P_{air}$, replacing P_{air} with $P_{droplet}$ yields $P_{liquid} < P_{droplet}$. This pressure difference inside the liquid creates a mass flow, filling the channel at a rate depending on the viscosity of the liquid and the hydraulic resistance of the channel. **(B)** Microscope images (after background subtraction) when (i) a PBS containing a red dye autonomously flows in a 200-µm-wide, 15-µm-deep channel ($P_{liquid}<<P_{air}$), (ii) the center of the meniscus gets pinned at the trench while the edges still slowly advance ($P_{liquid}<P_{air}$), (iii) the flow stops and the meniscus stays in its steady-state position ($P_{liquid}=P_{air}$), (iv) the center of the meniscus gets unpinned when 3 V potential difference is applied and temporarily (~0.5 s) gets pinned at the rising edge of the trench, and (v-vi) the liquid continues its flow ($P_{liquid}<<P_{air}$). **(C)** Microscope image showing the steady-state (ΔP = 0) profile of the liquid meniscus when it is pinned at the e-gate trench. Here, the meniscus forms a concave shape from the top view, which is compensated by a convex profile along the other axis (estimated from the darker area). In addition, the edges of meniscus towards the SU-8 channel walls form a multi-curvature shape to match the contact angle of SU-8 (~80° for water). **(D-E)** Plots showing the location of the meniscus estimated from the gray values from the color-inverted frames recorded during an electrogating experiments (Movie S1, figs. 3B and C). Plots show accumulated profiles for each frame along ROI lines at y=100 µm (channel center) and y = 190 µm (close to the channel wall).

Each line in the plots represents a frame (1/30 s) and different colors are used to highlight individual events (black: initial capillary flow, red: pinning, blue: temporary pinning after activating the e-gate, and green: resumed flow). After the application of 3 V, the center of the meniscus spontaneously moves to the rising edge of the 10-µm-wide trench while its edges remain anchored to the channel walls (can be seen in the insets with the magnified view). The meniscus gets temporarily (~0.5 s) pinned at this location (blue lines) and continues filling the channel (green lines). **(F)** ImageJ macro code written to generate the plots. Photo credit: Yuksel Temiz, IBM Research - Zurich

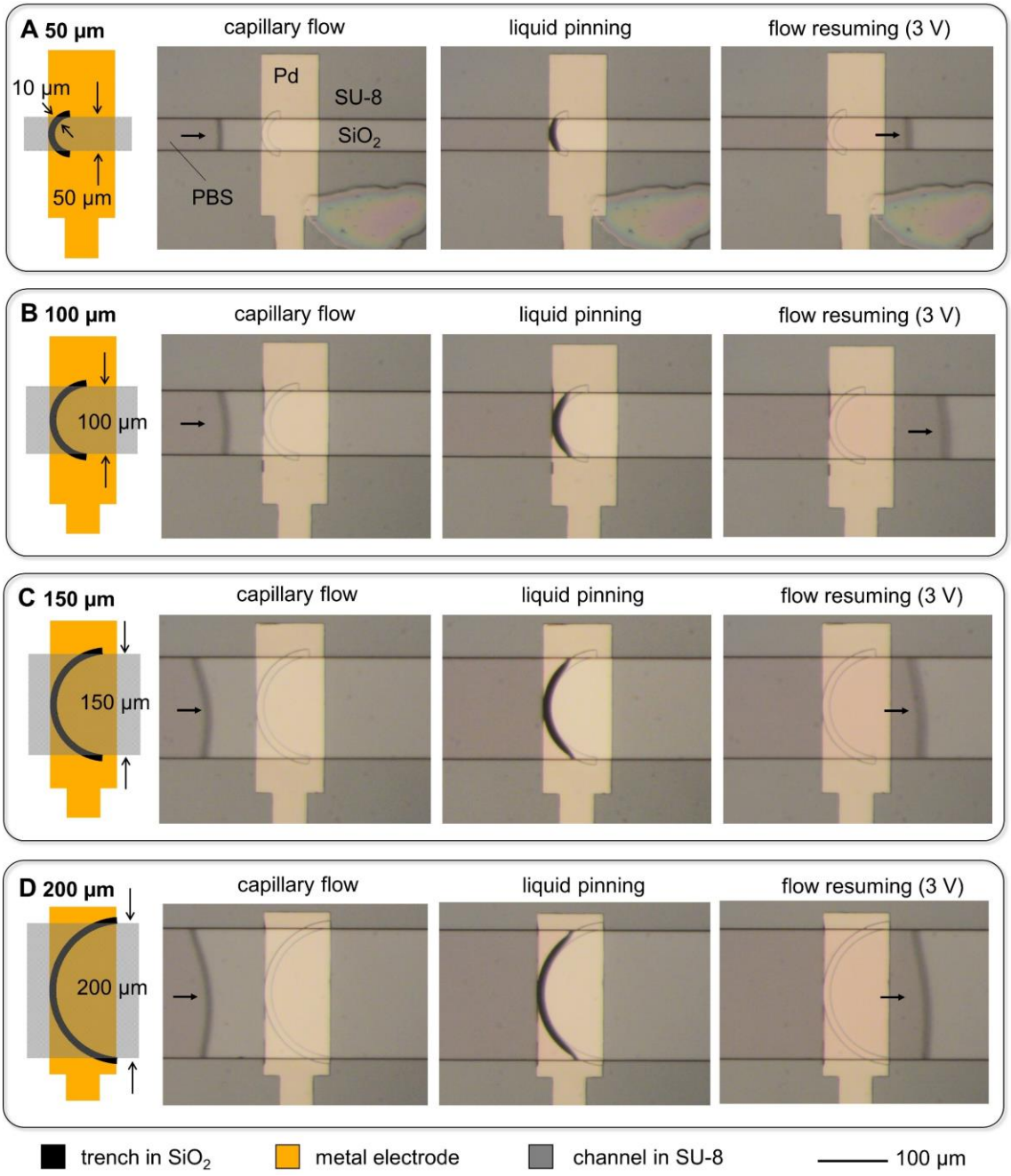

Fig. S4. Examples of e-gates having different widths and activated for stop-and-go flow control of PBS. Microscope images showing the flow of PBS in channels having a width of **(A)** 50 µm, **(B)** 100 µm, **(C)** 150 µm, and **(D)** 200 µm by capillary action (left), with pinning of the liquid at the semicircular trench etched in SiO_2 (middle), and after activation of the e-gates using a 3 V potential difference between the liquid (+) and the Pd electrode (ground) patterned over the trench (right). Layouts of e-gates are provided for clarity. Photo credit: Yuksel Temiz, IBM Research - Zurich

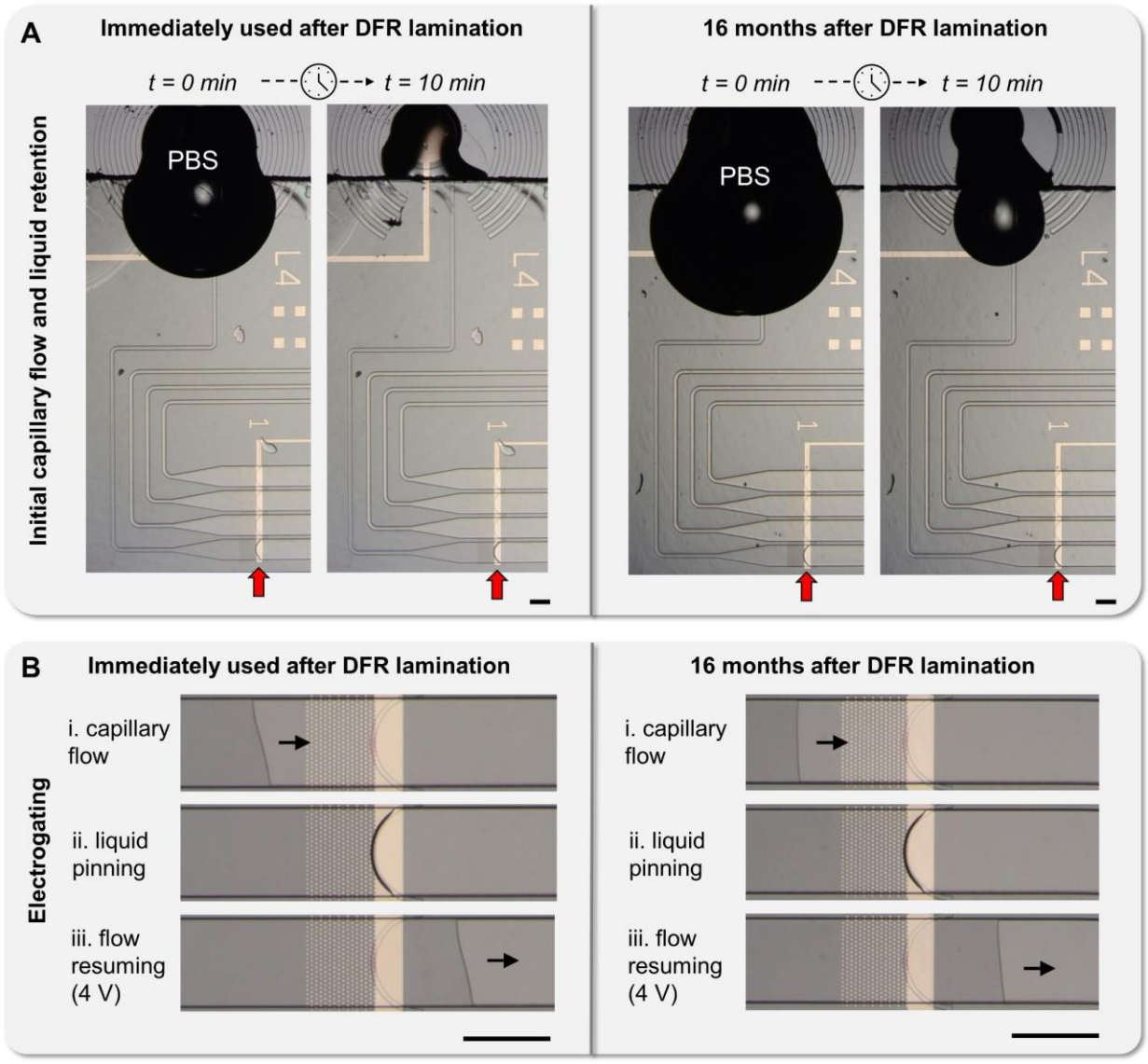

Fig. S5. Long-term storage tests using sealed chips stored in wafer boxes for 16 months. (A) Capillary-driven flow of PBS and its 10-min retention at an e-gate (red arrows) for chips used immediately after DFR lamination (left) and after 16 months of storage in dark (right). We did not observe any quantifiable effect of the storage on liquid retention when chips were kept in dark in an opaque wafer box. The initial liquid flow was slightly slower at the first few mm of the channel of the stored chip possibly due to some contamination from the air (e.g. organic contaminations). The chips kept in a transparent wafer box, however, failed to generate sufficient capillary pressure due to continuous exposure of the DFR to daylight, rendering the DFR less hydrophilic over time. **(B)** Experiments showing a very similar electrogating behavior between the chips used immediately after sealing (left) and used 16 months after sealing (right). (Scale bars: 200 µm). Photo credit: Yuksel Temiz, IBM Research - Zurich

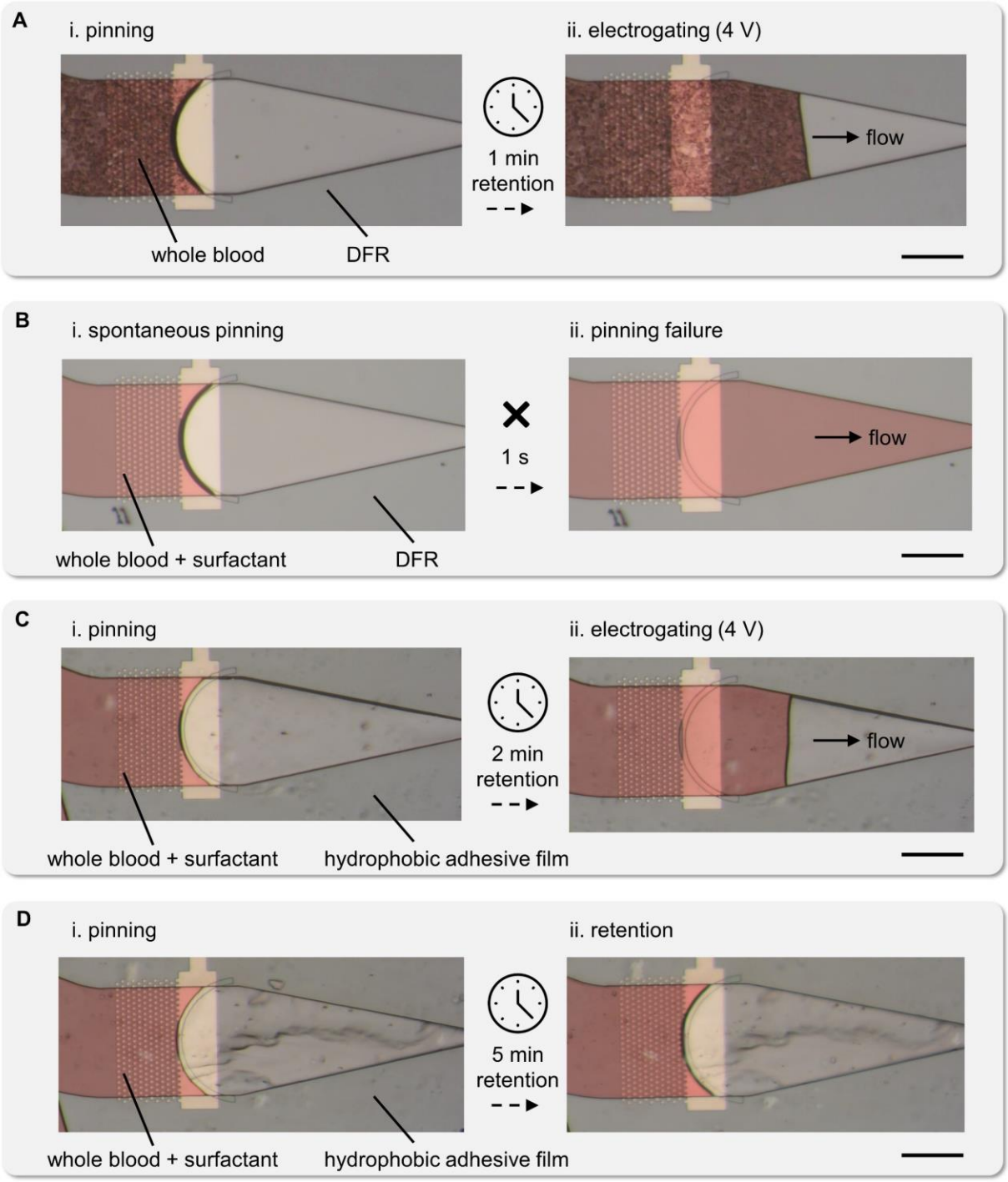

Fig. S6. Pinning and electrogating experiments using whole blood. (A) Stopping the capillary-driven flow of whole blood at an e-gate for 1 min and resuming the flow by applying 4 V to the e-gate electrode. DF-1050 DFR (Engineered Materials Systems, Inc.) with a water contact angle of ~70° was used as the top sealing layer. **(B)** The chips with DF-1050 DFR failed to pin whole blood containing 10 mM Triton X-100 surfactant in PBS, which is a common solution used to lyse red blood cells. To address this issue, a hydrophobic adhesive film (ARseal 90880, Adhesives Research, Inc.) with a silicone-based pressure-sensitive adhesive was tested successfully for **(C)** electrogating and **(D)** a retention time of 5 min. Longer retention times could not be tested because the 3 µL sample applied to the loading pad became viscous by evaporation. Also, long-term stability of this hydrophobic film was not evaluated. (Scale bars: 100 µm). Photo credit: Yuksel Temiz, IBM Research - Zurich

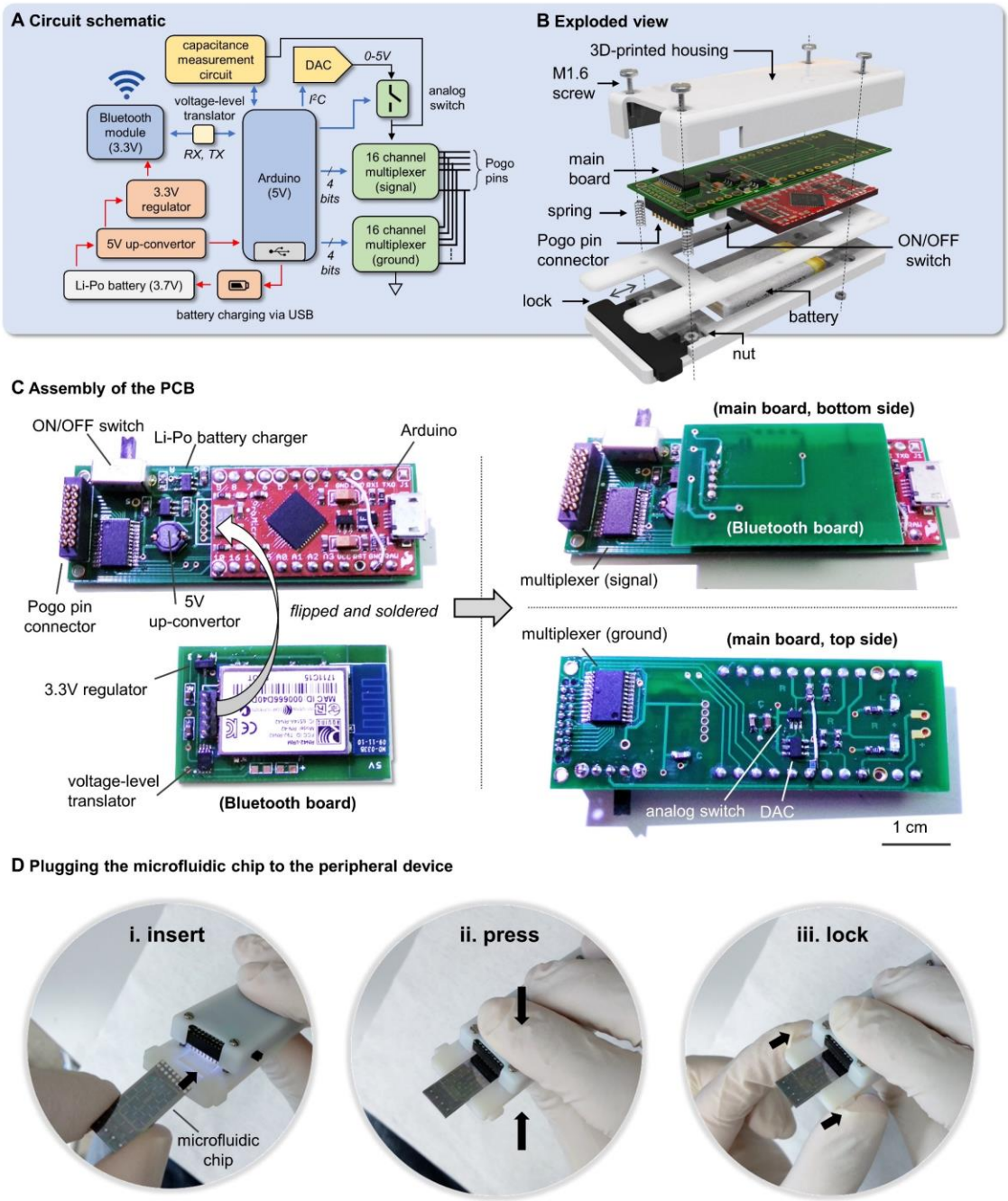

Fig. S7. Design and implementation of the portable peripheral device used for e-gate activation and flow monitoring. (A) Simplified circuit schematic of the peripheral device comprising an Arduino microcontroller (5 V), a Bluetooth module (3.3 V), a 12-bit digital-to-analog converter (DAC) to generate voltages for e-gates that can be tuned from 0 to 5 V in ~1.2 mV steps, two 16-channel multiplexers to select positive and ground contacts respectively, a capacitance measurement circuit using a charging resistor (10 MΩ) and a discharging resistor (1 KΩ), an analog switch to select either the electrogating mode (i.e. applying a voltage) or flow monitoring mode (i.e. measuring the capacitance), a 3.7 V lithium polymer battery and its charging circuit, and voltage regulators to generate 5 V and 3.3 V. **(B)** 3D-rendered exploded view of the device showing the arrangement of the components fitting in a 70 × 12 × 25 mm^3 3D-printed housing. **(C)** Photographs of the printed circuit boards (PCBs) where the PCB carrying the Bluetooth module and its voltage regulator was flipped and soldered on top of the main board, which carries the 16-contact Pogo pin connector, the Arduino microcontroller and other electronic components. **(D)** The operation of the device involves (i) insertion of the microfluidic chip, (ii) pressing the spring-loaded top part of the device to ensure electrical connection between the chip and the Pogo pin connector, and (iii) locking the top part using a laterally-movable piece blocking the nuts. Photo credit: Yuksel Temiz, IBM Research - Zurich

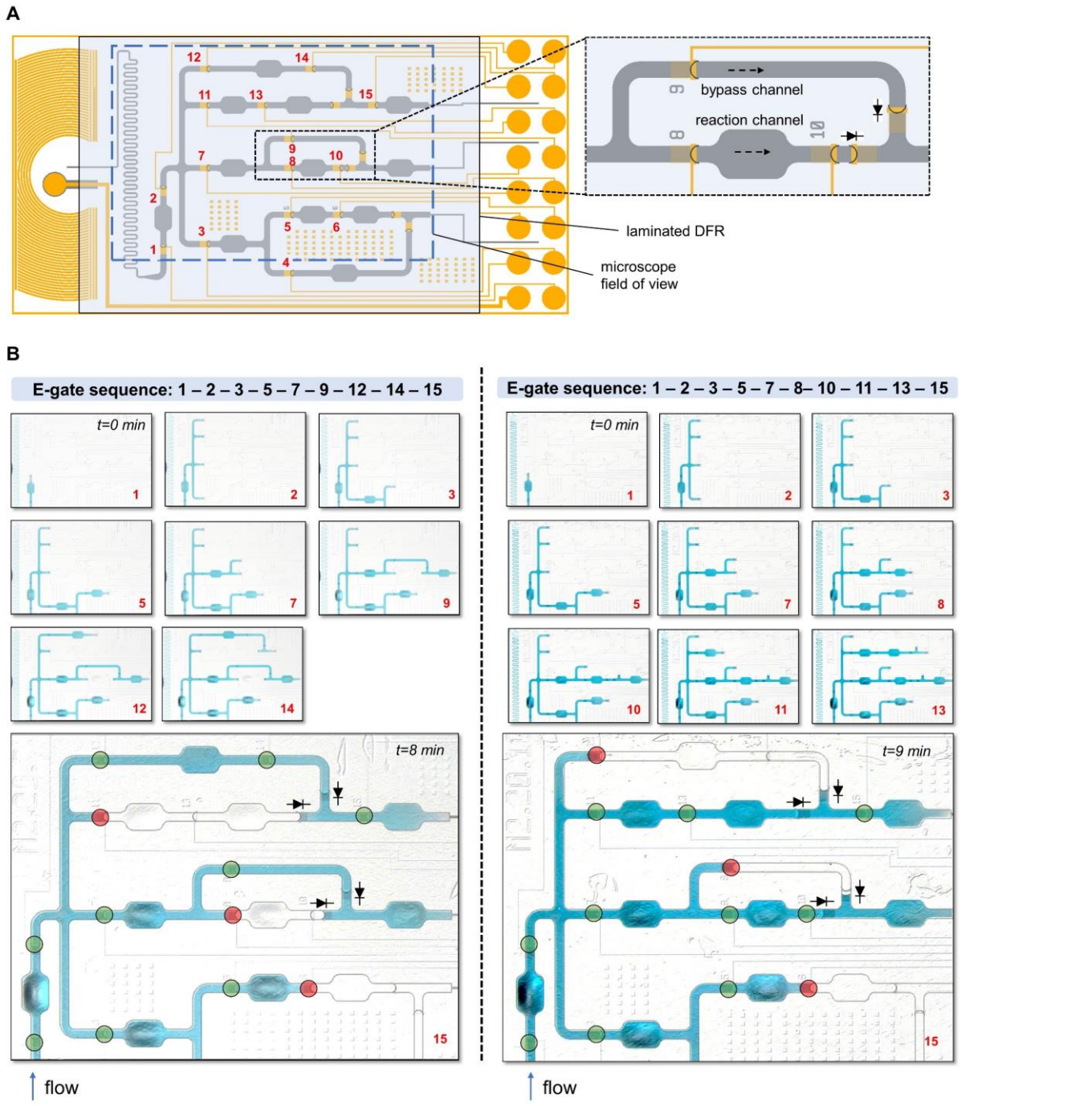

Fig. S8. Generating variants of flow paths using a generic chip design. (A) Example of a chip layout comprising multiple options of flow paths, which can be selected using e-gates. The inset shows a design where the flow can be directed to a reaction channel (e.g. channel with integrated reagents) or to a bypass channel depending on the application. An e-gate placed at the outlet of the reaction chamber (e.g. e-gate #10) can be used to time the reaction. Passive e-gates (i.e. pinning structures without electrical contacts) can be used as "diodes" to prevent undesired backflow. **(B)** Microscope images showing results from two identical chips applied with different electrogating sequences. A snapshot image was captured every minute after activating an e-gate manually from the smartphone application (green and red circles highlight the e-gates that have been activated or not, respectively). Photo credit: Yuksel Temiz, IBM Research - Zurich

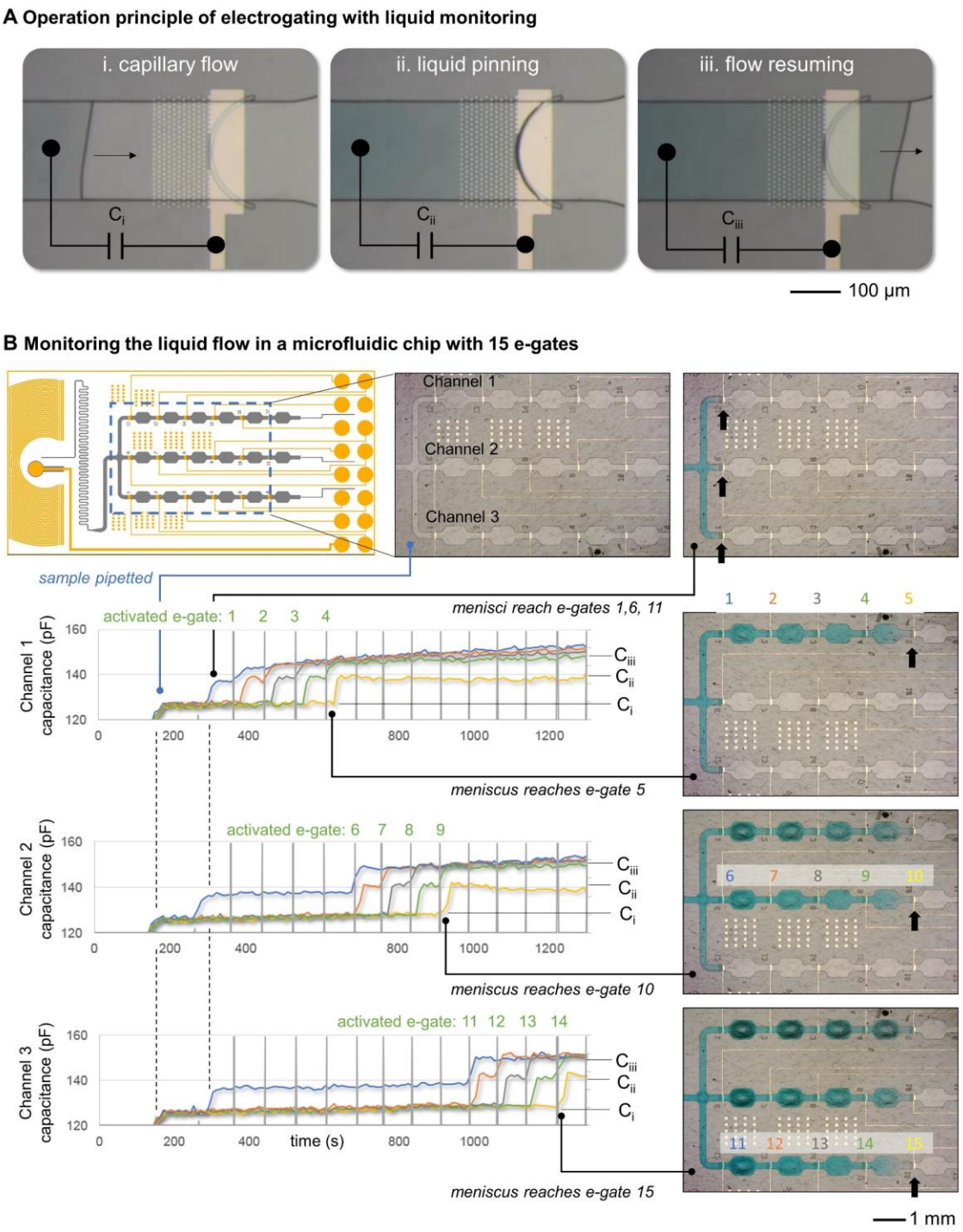

Fig. S9. Electrogating combined with liquid monitoring. (A) Microscope images showing the operation principle of liquid monitoring based on the capacitance of electrodes. (i) The e-gate electrode is initially dry, (ii) gets partially wet when the liquid is pinned at the trench, and (iii) the surface of the electrode in contact with the liquid increases when the flow is resumed, leading to higher capacitance. **(B)** An experimental result showing the change in the capacitance for a chip with 3 parallel channels and 15 e-gates in total. E-gates were sequentially activated every minute and their capacitances were measured every second and plotted for individual channels. The capacitance was about 125 pF when the e-gates were dry (C_i), reached 140 pF when the liquid was pinned (C_{ii}) and increased to 145-150 pF after activation of the e-gate. The capacitances of e-gates # 5, 10, and 15 stayed as expected at 140 pF (C_{ii}) because they were not activated. Microscope images show the location of the liquid meniscus (black arrows) when it reaches to the first and the last e-gates for each channel. Photo credit: Yuksel Temiz, IBM Research - Zurich

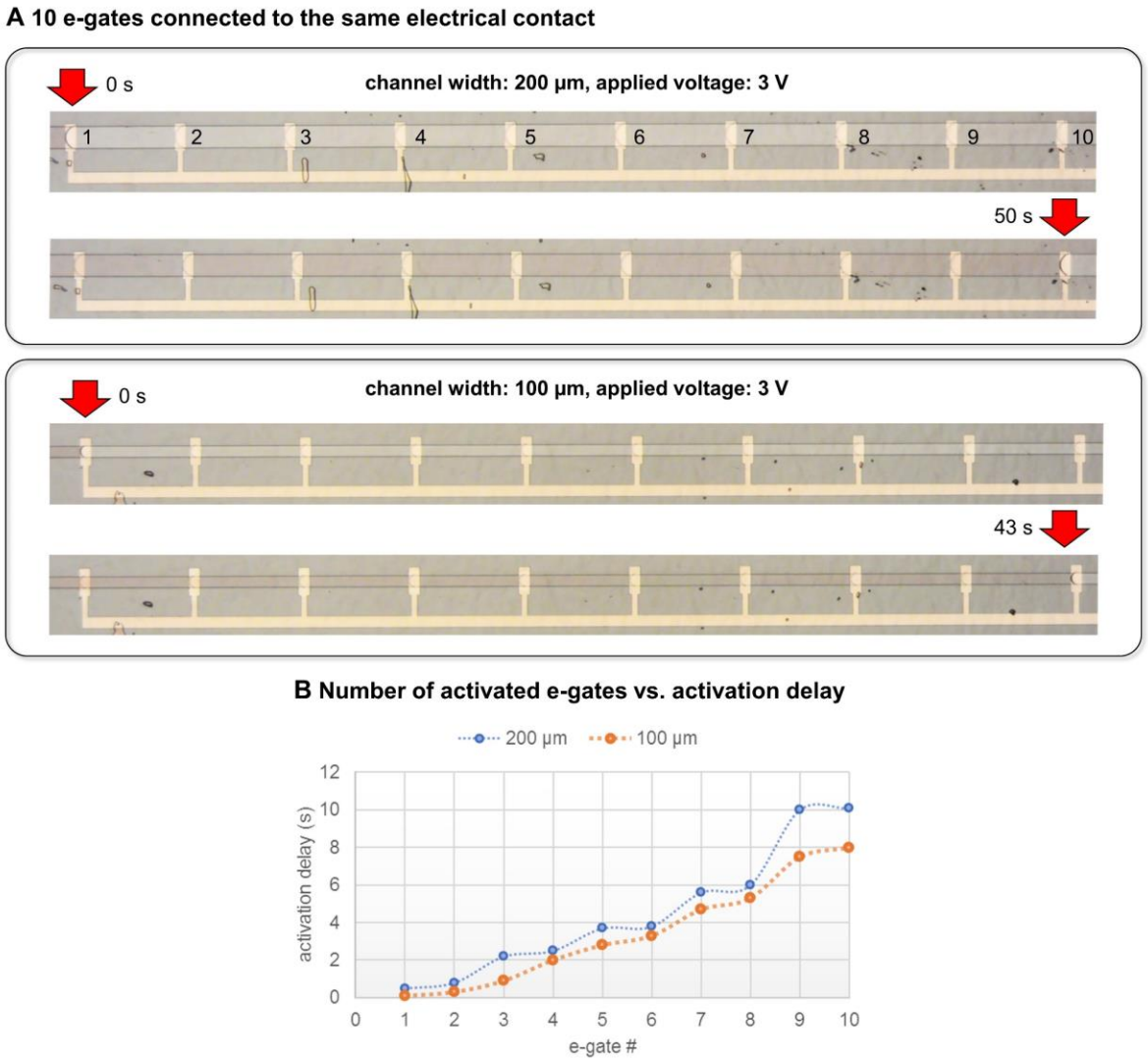

Fig. S10. Ten e-gates connected in parallel. (A) Microscope images showing 10 e-gates connected to the same electrical contact and the flow of PBS in 200 µm (top) and 100 µm (bottom) channels. A potential difference of 3 V was continuously applied between the liquid and the e-gates while recording the liquid flow (red arrows show the location of the liquid meniscus). **(B)** Plot showing the e-gate activation delay extracted from the video. The delay was less than 1 s for two e-gates connected in parallel while it increased to 10 s for the 10th e-gate. The delay in 100-µm-width channels was slightly less than that in 200-µm-width channels probably because smaller e-gates are less stable, and their electrical capacitance is lower (i.e. lower RC time constant). Photo credit: Yuksel Temiz, IBM Research - Zurich

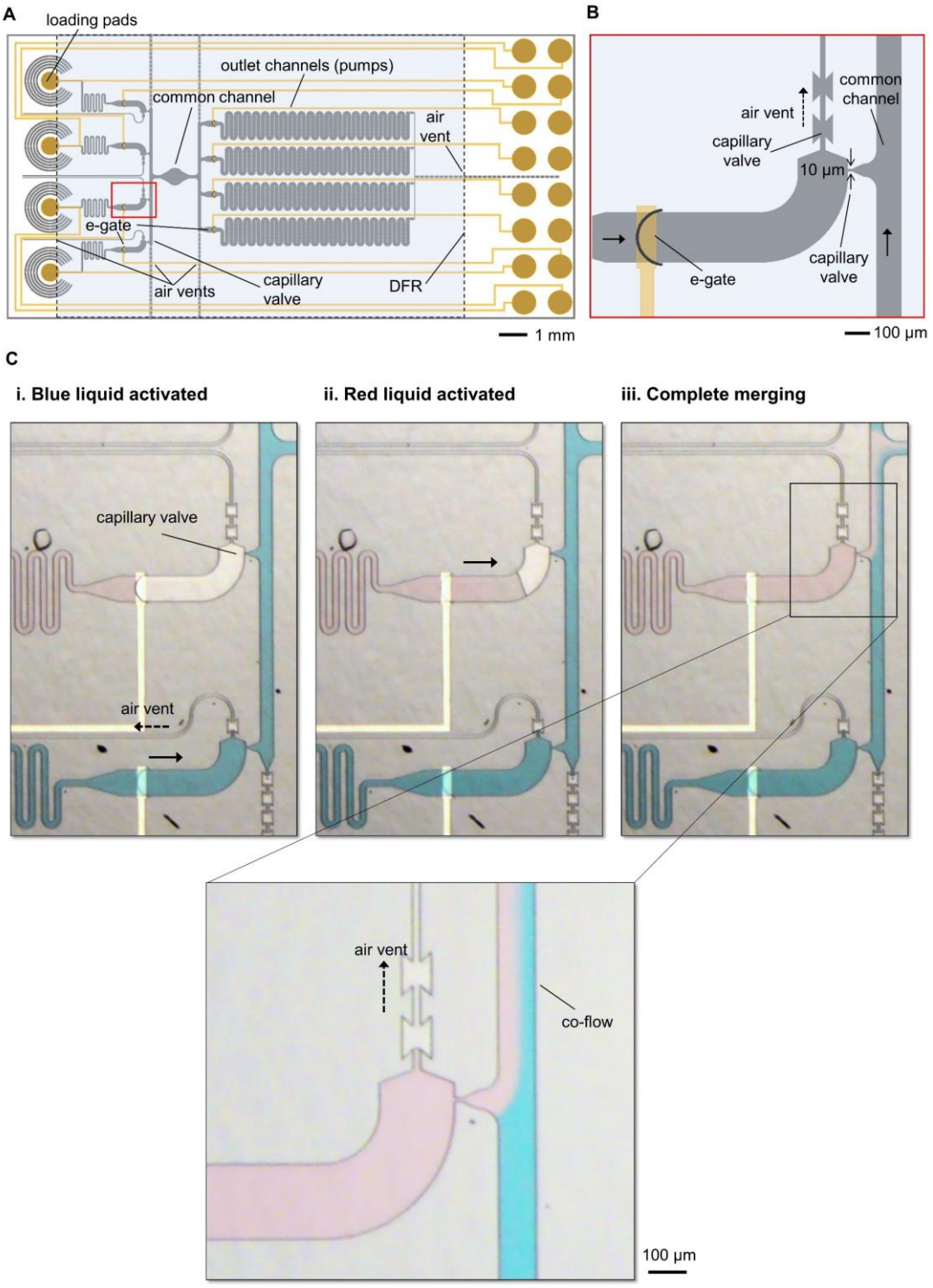

Fig. S11. Controlling the flow of multiple liquids through a common channel using e-gates and capillary valves with vents. (A) Layout of a chip design allowing the flow of four pipetted liquids through the same channel in any sequence or combination. The chip uses four loading pads, four vented capillary valves controlled by e-gates, and additional e-gates to control the flow in four outlet channels. **(B)** Layout of the capillary valve with a vent that enables the merging of two liquids without creating an air bubble. **(C)** Experimental results showing the operation of such a valve where (i) the liquid in blue flows in the common channel, (ii) the liquid in red is activated, and (iii) complete merging is achieved by pushing the air out through the vent. Photo credit: Yuksel Temiz, IBM Research - Zurich

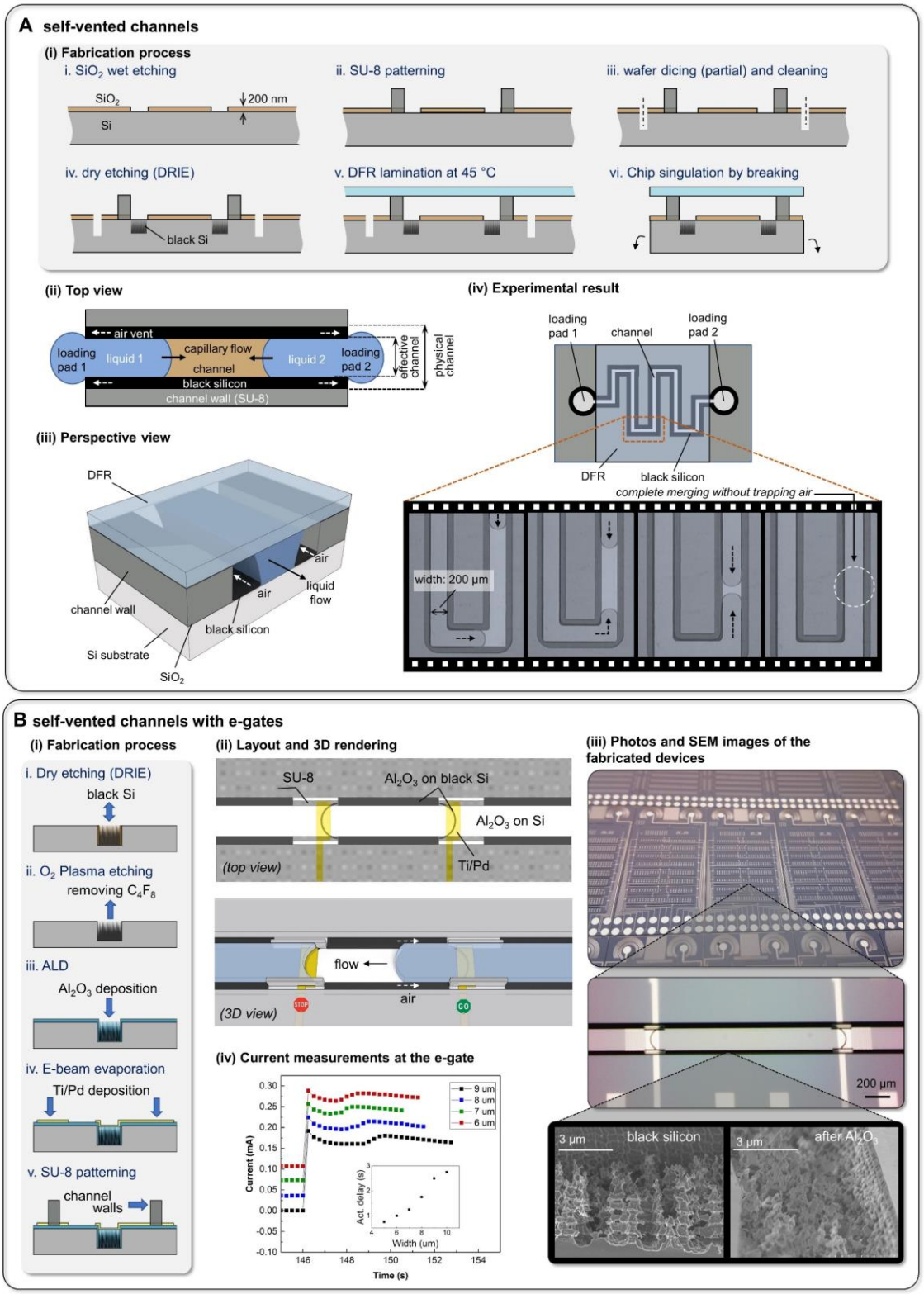

Fig. S12. Self-venting mechanism in microfluidic channels and its integration with e-gates. (A) Operation principle and experimental results of a self-venting mechanism in a microfluidic channel using black silicon. (i) Schematic representation (not to scale) of the fabrication process for creating self-vented channels. (ii) Top view showing the components of the microfluidic channel and the black silicon hydrophobic areas to merge two liquid fronts without creating an air bubble in between. (iii) 3D representation of the channel

indicating the vent areas formed between the liquid and the channel walls. (iv) The top view of an experimental design for demonstrating self-venting in a microfluidic channel and microscope images showing the merging of two liquid fronts using the action of self-venting without formation of bubbles. **(B)** Implementation of e-gates using black silicon for an integrated system including self-venting. (i) Schematic representation (not to scale) of the fabrication process for creating e-gates based on black silicon patterning. (ii) Layout of a self-vented channel with two e-gates (top) and its 3D rendering to illustrate the merging of two liquids (bottom). (iii) Photographs of the fabricated wafer (top), self-vented channel with e-gates using black silicon (middle) and SEM images of microstructures from the black silicon area: after 2 min DRIE process (image on the bottom left) and further after deposition of an Al_2O_3 layer (image on the bottom right). (iv) Characteristic current vs. time curves during activation of the e-gate for a different width of the black silicon area. Inside is the activation delay time of the gate as a function of the width. Photo credit: Yulieth Arango and Yuksel Temiz, IBM Research - Zurich

Supplementary Movies:

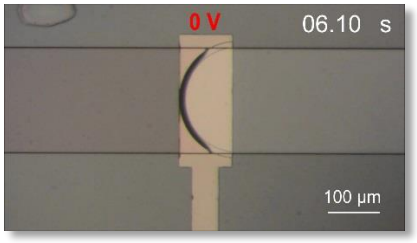

Movie S1. Video captured using a microscope to demonstrate the operation of an e-gate during the capillary filling of a 200-µm-wide, 15-µm-deep microfluidic channel with PBS. The first half of the video is in real-time and the second half shows the pinning of the liquid at the e-gate trench and resuming the flow frame by frame after background subtraction. Movie credit: Yuksel Temiz, IBM Research - Zurich

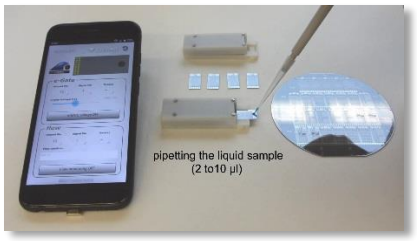

Movie S2. A typical workflow of using capillary-driven microfluidic chips with programmable liquid circuits. A chip is inserted to a portable device and the electrical connection to 16 contacts is achieved using a spring-loaded Pogo pin connector. The flow of a pipetted liquid (or multiple liquids) is controlled and monitored using an app that communicates with the peripheral device via Bluetooth. Movie credit: Yuksel Temiz, IBM Research - Zurich

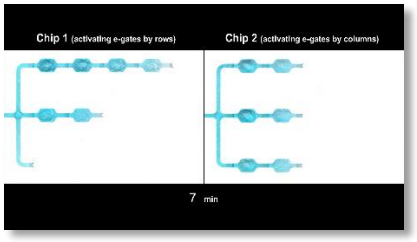

Movie S3. Two microfluidic chips with identical designs but programmed for the activation of e-gates in different sequences. The second part of the movie shows the capillary-driven flow of PBS and the electrogating in real-time. Movie credit: Yuksel Temiz, IBM Research - Zurich

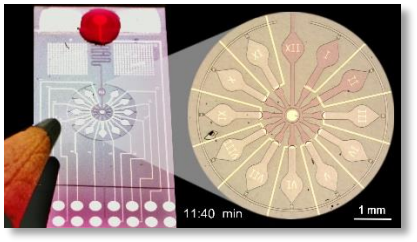

Movie S4. A "microfluidic clock" that works autonomously according to a protocol applied from a smartphone. PBS with red dye fills microfluidic channels controlled by e-gates, representing hands of a clock. E-gates are automatically activated every 5 min by applying 3 V for 3 s according to the protocol. Movie credit: Yuksel Temiz, IBM Research - Zurich

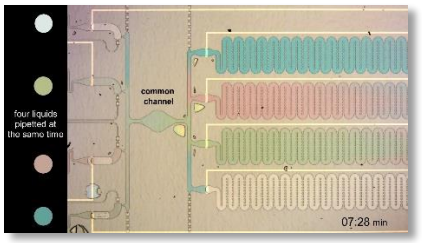

Movie S5. Sequential flow of four pipetted liquids (PBS with blue, red, green dyes and no dye) through a common channel. An incoming liquid merges to a common channel, which is already filled with another liquid, owing to capillary valves with air vents. The flow of a previously activated liquid is stopped by generating an air bubble by applying a reverse potential to e-gates electrodes. Movie credit: Yuksel Temiz, IBM Research - Zurich

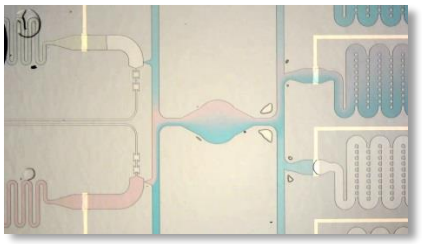

Movie S6. Creating a co-flow of two liquids using capillary valves with air vents and e-gates. At the beginning of the video, PBS in red and blue flow together, then PBS in green is activated and the flow of PBS in blue is stopped. Movie credit: Yuksel Temiz, IBM Research - Zurich

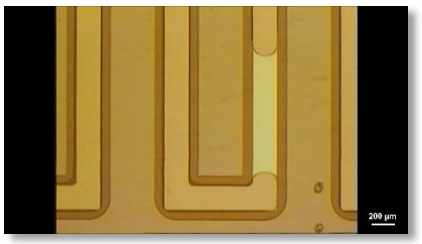

Movie S7. Two menisci of PBS flowing in opposite directions and merge without trapping an air bubble owing to self-vented channels. Movie credit: Yuksel Temiz, IBM Research - Zurich

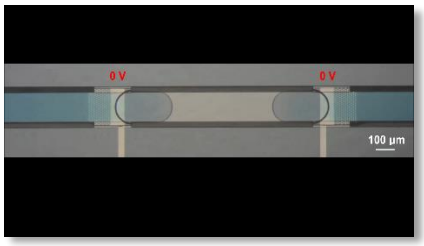

Movie S8. Synchronized merging of two liquid menisci (PBS with a blue dye) using e-gates with a trench patterned in black silicon and self-vented channels. The menisci merge without creating an air bubble owing to the displacement of air sideway along the black silicon stripes. Movie credit: Yuksel Temiz, IBM Research - Zurich